Coherency-Broken Bragg Filters: Overcoming On-Chip Rejection Limitations

Dorian Oser, Florent Mazeas, Xavier Le Roux, Diego Pérez-Galacho, Olivier Alibart, Sébastien Tanzilli, Laurent Labonté, Delphine Marris-Morini, Laurent Vivien, Éric Cassan, et al.

Coherency-Broken Bragg Filters: Overcoming On-Chip Rejection Limitations

*Dorian Oser, Florent Mazeas, Xavier Le Roux, Diego Pérez-Galacho, Olivier Alibart, Sébastien Tanzilli, Laurent Labonté, Delphine Marris-Morini, Laurent Vivien, Éric Cassan, and Carlos Alonso-Ramos**

Selective optical filters with high rejection levels are of fundamental importance for a wide range of advanced photonic circuits. However, the implementation of high-rejection on-chip optical filters is seriously hampered by phase errors arising from fabrication imperfections. Due to coherent interactions, unwanted phase-shifts result in detrimental destructive interferences that distort the filter response, whatever the chosen strategy (resonators, interferometers, Bragg filters, etc.). State-of-the-art high-rejection filters partially circumvent the sensitivity to phase errors by means of active tuning, complicating device fabrication and operation. Here, a new approach based on coherency-broken Bragg filters is proposed to overcome this fundamental limitation. Non-coherent interaction among modal-engineered waveguide Bragg gratings separated by single-mode waveguides is exploited to yield effective cascading, even in the presence of phase errors. This technologically independent approach allows seamless combination of filter stages with moderate performance free of active control, providing a dramatic increase of on-chip rejection. Based on this concept, on-chip non-coherent cascading of Si Bragg filters is experimentally demonstrated, achieving a light rejection exceeding 80 dB, the largest value reported for an all-passive silicon filter.

1. Introduction

The silicon-on-insulator (SOI) platform allows realizing miniaturized optical circuits that can be fabricated in existing CMOS facilities. These high-performance photonic devices have a great potential for a plethora of applications, including datacom,[1] sensing,[2,3] and quantum information.[4,5] While many highly efficient components have already been demonstrated in the silicon photonics platform, for example, fiber-chip couplers,[6] fast modulators,[7] and photodetectors,[8] the realization of high-rejection wavelength filters remains challenging. Indeed, the lack of on-chip optical filters with strong rejection hinders the full integration of some advanced nonlinear circuits. One clear example is silicon photon-pair sources, with a great potential for applications in quantum key distribution[9] and optical quantum computing.[4] These sources harness spontaneous four-wave mixing in Si micro-ring resonators to generate multispectral entangled photon-pairs from a strong optical pump.[5,10–12] However, due to the substantially higher pump intensity compared to that of the photon-pairs, such Si-based sources require on-chip rejections exceeding 100 dB.[13] This stringent rejection requirement lies beyond the capabilities of current Si wavelength filters, precluding full integration of Si-based photon-pair sources. Pump rejection has been demonstrated in silicon chips combining a high-performance Bragg filter (65 dB rejection) and a ring resonator (30 dB rejection).[14] Still, this solution requires cascading two identical chips to achieve effective rejection of the pump. The main reason for this is the limited rejection achieved by state-of-the-art on-chip Bragg filters.

A myriad of optical filters has been reported for the silicon photonics technology, including Bragg grating filters,[15–17] cascaded micro-resonators,[18,19] and Mach–Zehnder interferometers (MZI).[20,21] Although theoretical designs can achieve remarkably large rejection levels, most practical implementations are limited to the 30–60 dB range.[15–23] The main limiting factor to the achievable on-chip optical rejection currently lies in fabrication imperfections. More specifically, the high-index contrast of the SOI platform makes these circuits very sensitive to fabrication errors, as small deviations in waveguide width and height strongly affect the propagation constant of light, resulting in large phase errors.[24] This detrimental effect distorts the

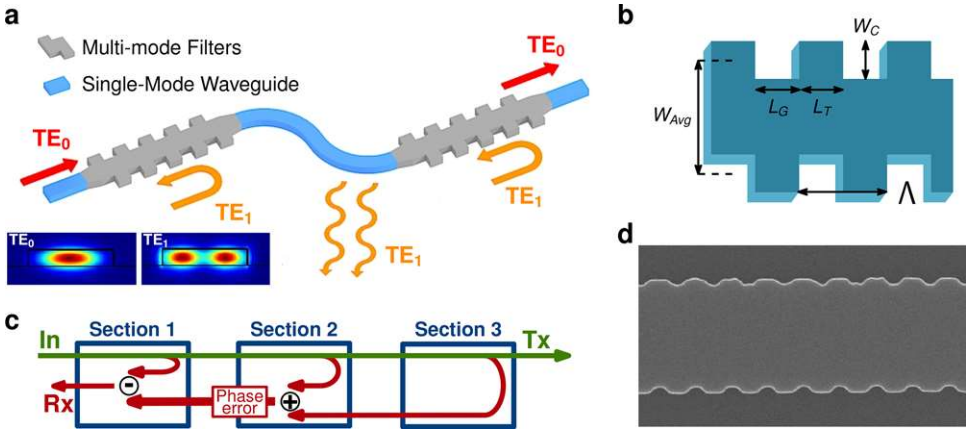

Figure 1. a) Schematic view of proposed cascaded filter. Fundamental mode (TE_0) is back-reflected into first-order mode (TE_1). Single-mode waveguide sections separating adjacent filters radiate the back-reflected TE_1 mode away, precluding coherent interaction among different stages. b) Schematic of shifted Bragg geometry providing Bragg back-reflections in higher-order TE_1 mode. c) Block diagram illustrating the detrimental effect of phase errors in cascaded Bragg gratings with coherent interaction. d) Scanning electron microscopy (SEM) image of a fabricated shifted grating.

filter response, thus compromising its rejection capability. In the case of cascaded multistage filters, relative phase errors may result in destructive interferences or relative wavelength shifts that offset the benefits of cascading. These interference effects have been minimized in optical fibers[25–27] and Si chips[28] by cascading grating sections with different Bragg resonance wavelengths. Although effective for dispersion compensation or tuning of the filter bandwidth, this strategy does not overcome rejection depth limitations as each grating section reflects in a different wavelength range. On the other hand, multistage filters combining nominally identical ring resonators or MZI sections are strongly affected by fabrication imperfections, as phase errors actually shift the wavelength response of each filter section offsetting the benefits of the cascading. The wavelength of the notch in ring resonators and MZIs is determined by the total phase accumulated along the full optical path. Then, any punctual waveguide error can alter the accumulated phase, shifting the wavelength of the notch. These drawbacks have been partially alleviated by implementing active phase-tuning in multistage filters.[13,14,29,30] For instance, 60 dB rejection has been shown on a single chip with cascaded Mach–Zehnder interferometers (MZI),[13] and 100 dB has been demonstrated for a tenth order micro-ring-based filter.[29] Still, this approach complicates device fabrication and operation, as it requires implementation of tuning circuitry and continuous monitoring of the filter response to maintain proper performance.

Here, we present a new strategy for the on-chip implementation of high-rejection multistage filters, free of active circuit control. The proposed approach, schematically depicted in **Figure 1**a,b, exploits modal engineering in waveguide Bragg gratings to achieve non-coherent cascading, making the device immune to relative phase errors among the stages. It turns out that such strategy permits overcoming one of the major limitations of on-chip filters. The waveguide gratings are shaped to yield Bragg back-reflections propagating in a high-order spatial mode. These back-reflections are radiated away in single-mode waveguides interconnecting adjacent filter stages, precluding coherent interaction. This generic strategy allows the implementation of high-rejection filters by all-passive cascading of modal-engineered Bragg gratings with relaxed performance requirements. Hence, the broken-coherency Bragg filter approach proposed here opens a completely new route for the implementation of high-performance on-chip optical filters.

2. Experimental Section

The different sets of shifted Bragg filters were fabricated in SOI wafers comprising a 220 nm thick silicon and a 2 µm buried oxide layer, using an electron beam lithography (Nanobeam NB-4 system 80 kV) with a step size of 5 nm. Dry and inductively coupled plasma etching (SF_6/C_4F_8) were used to define the patterns. We used a tunable laser source from Yenista, providing 10 dBm output power around 1550 nm wavelength. A polarization rotator was used to set transverse-electric (TE) polarization at the input grating. No external polarization filter was used. To collect the filter spectra, we used automatic high-resolution wavelength scan with Yenista CT400 (noise floor of about −75 dBm) and point-by-point scan with optical spectrum analyzer (OSA Anritsu MS9710B, with noise floor near −90 dBm).

3. Results and Discussion

Waveguide Bragg gratings reflect light back into the input waveguide by constructive interference of partial reflections in each period.[31] This resonant back-reflection occurs when the Bragg phase-matching condition, $\lambda_o = \Lambda 2n_{eff}/p$, is satisfied. Here, λ_o is the Bragg resonance wavelength, Λ the grating period, n_{eff} the effective index of the mode propagating through the grating, and p is the Bragg order. On the other hand, from coupled mode theory, it is known that the rejection (R) and bandwidth ($\Delta\lambda$) of the filter are related to the grating geometry and filter length (L_F) by[36]

$$R = \tanh^2(\kappa L_F) \tag{1}$$

$$\Delta\lambda = \frac{\lambda_0^2}{\pi n_g}\sqrt{\kappa^2 + \frac{\pi^2}{L_F^2}} \tag{2}$$

Note that the group index (n_g) and the coupling coefficient (κ) here are mainly governed by the grating geometry. Ideally, arbitrarily large rejections can be achieved just by implementing a strong coupling coefficient or a sufficiently long filter. In practice, achievable rejection saturates beyond a certain filter length.[15–17] To achieve the theoretical rejection level, partial reflections in all periods of the filter have to interfere constructively. Punctual phase errors in the grating do not have an important effect on the total resonant wavelength as they do not affect the resonant wavelength of other periods. However, even very small fabrication imperfections alter the phase along the filter, distorting the constructive interference. Such errors accumulate with increasing filter length, setting the saturation level. Cascading conventional Bragg filters does not address this issue. Conventional cascaded Bragg gratings interfere coherently. This is indeed the principle harnessed in Fabry–Perot cavities.[32–34] Thus, rejection in cascaded Bragg filters may be degraded by destructive interferences due to the phase shift induced by propagation through the interconnecting waveguide (see Figure 1c). Even if this waveguide had the optimal length and width to induce a phase shift producing a constructive interference (i.e., free of fabrication imperfections), back-reflections from each stage still need to propagate in phase through the previous gratings. This has two detrimental consequences: first, the effectiveness of cascading is affected by relative phase shifts between stages; second, fabrication imperfections in each section distort back-reflections generated by the following sections. To overcome this limitation, we propose a new multistage filter strategy combining multimode Bragg gratings and single-mode interconnection waveguides (see Figure 1a). The Bragg gratings are designed to yield back-reflections propagating in the first higher-order mode. Then, back-reflections are radiated away in the single-mode interconnection waveguide section, avoiding propagation through previous gratings. This way coherent interaction among filter stages is precluded, circumventing the detrimental effect of cumulative phase errors, thus achieving effective cascading.

To consider that the reflection in one filter is not distorted by all other filters of the cascaded geometry, it is necessary to ensure that the reflection in this filter is substantially larger than the sum of all reflections arriving from the following filters. The reflection in the first filter will be called signal (S), while the sum of the reflection in all other filters, arriving to the first filter, will be called interference (I). As schematically shown in the inset of **Figure 2**a, the signal and interference can be calculated as

$$S = P_{IN} R \tag{3}$$

$$I = P_{IN} R \sum_{n=2}^{N} (1 - R)^{2n-3} \alpha^{n-1} \tag{4}$$

where α is the radiation ratio, P_{IN} the incident power, and N is the total number of cascaded gratings. Figure 2a shows the signal to interference ratio calculated as a function of α for different values of the power reflectivity R of each grating. It can be seen that radiation ratios of 20 and 30 dB yield at least 2 and 3 orders of magnitude difference between the signal and the interference, respectively, thereby precluding distortion of the reflection in the first filter.

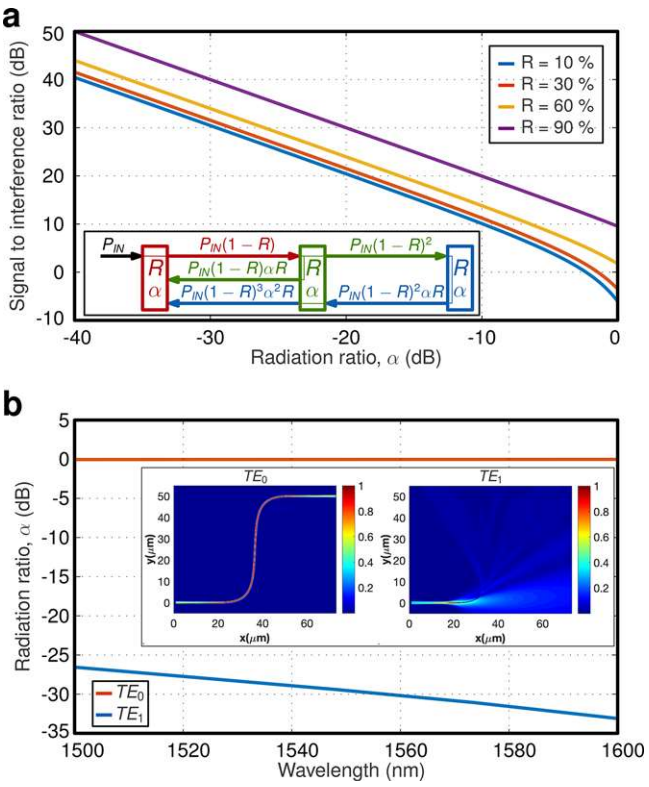

Figure 2. a) Signal to interference ratio calculated from Equations (3) and (4) as a function of the radiation radio, α, for different values of the reflectivity (R). b) Radiation ratio, α, calculated with 2.5D-FDTD (see ref. [35]) when the fundamental and first-order modes are injected in the proposed interconnection section, comprising 25-μm-long tapers, S-bends with 15 μm radius, and single-mode straight waveguide section with 20 μm length. Insets show the propagation for the fundamental (left panel) and first-order mode (right panel) at 1550 nm wavelength.

To radiate the first-order-mode reflection, we introduce tapers to single-mode waveguide, and a cosine-shaped S-bend with a central straight waveguide section. Both the S-bend and the straight section are implemented with a single-mode waveguide. We chose a waveguide width of 400 nm, providing single-mode behavior. This interconnection section should also provide low insertion loss for the fundamental mode outside the rejection band to avoid degrading the total filter rejection. Hence, 25-μm-long linear tapers are implemented between the filter and the single-mode waveguide to achieve adiabatic transition, thus minimizing the loss for the fundamental mode and the transference of energy among modes. On the other hand, a 15 μm radius is used in the S-bend to minimize bending loss for the fundamental mode. Figure 2b shows the radiation ratio for the fundamental and first-order modes calculated using commercial 2.5D finite-difference time domain (FDTD) tool,[35] considering a central waveguide section with 20 μm length. The proposed interconnection section yields a loss of only −0.05 dB for the fundamental mode and a radiation ratio in excess of −25 dB for the first-order one, thereby ensuring negligible interference among cascaded gratings. As an example, the insets in Figure 2b show the propagation for the fundamental (left panel) and first-order mode (right panel) at 1550 nm wavelength.

From coupled mode theory, the rejection of conventional filters ideally scales with the length following Equation (1). However, our broken-coherency cascaded filter follows a different law and behavior, where each section is independent from the others and the rejections are accumulated

$$R = \left[\tanh^2(\kappa L_S)\right]^{N_S} \tag{5}$$

where L_S is the section length and N_S is the number of sections. For a given length and coupling coefficient, κ, this law yields a weaker rejection in the ideal case. However, we show experimentally that the resilience to phase errors in the broken-coherency approach allows substantial rejection improvement in practical implementations.

To demonstrate the broken coherency concept, we used SOI substrate with 220-nm-thick guiding Si layer. For the implementation of the multimode Bragg grating, we selected a fully etched process and a shifted-teeth geometry, as presented in Figure 1b. The grating lattice is defined by the average waveguide width (W_{Avg}), the corrugation depth (W_C), the length of the teeth (L_T) and gaps (L_G), and the period ($\Lambda = L_T + L_G$). By shifting the corrugation in one side of the grating half a period with respect to the other, this grating geometry precludes Bragg reflections in the fundamental mode,[37] while providing the asymmetry required to excite Bragg back-reflections in the first higher-order mode.[38]

We designed the shifted Bragg grating to operate with TE polarized light near 1550 nm wavelength using modal analysis and FDTD tools from commercial software.[35] The proposed design has a period Λ of 290 nm, an average waveguide width W_{Avg} of 1150 nm, a corrugation W_C of 50 nm, and a duty cycle of 50% ($L_T = L_G = 145$ nm). Note that this design is compatible with state-of-the-art immersion lithography. The period of 290 nm ensures a spacing between teeth larger than 100 nm, well within the capabilities of standard deep-UV lithography.[39] Although technologically feasible,[40,41] the 50-nm-wide corrugation may be challenging to implement with standard deep-UV lithography.

Figure 1d shows the scanning microscope image of one of the gratings. It can be noticed that the filter teeth are rounded, with local defects. We verified by simulation that rounding of the grating teeth does not affect the operation principle of the proposed filter. However, as discussed before, the local defects (different rounding among teeth, lateral roughness, etc.) alter the phase of the light propagating through the grating, distorting the experimental filter response.

Subwavelength fiber-chip grating couplers were used to inject and extract the light from the chip with cleaved single-mode (SMF-28) optical fibers.[42,43] These grating couplers were optimized to minimize back-reflections for the TE polarized light, thereby minimizing the Fabry–Perot ripples in the measurements for proper analysis of transmission spectra of the filters. Due to non-perfect polarization alignment at the input fiber, some residual light with transverse-magnetic (TM) polarization can propagate through the grating limiting the measured rejection. Thus, air is used as top cladding as a simple way to remove TM light. Similar functionality could also be achieved with on-chip polarization splitter.[44]

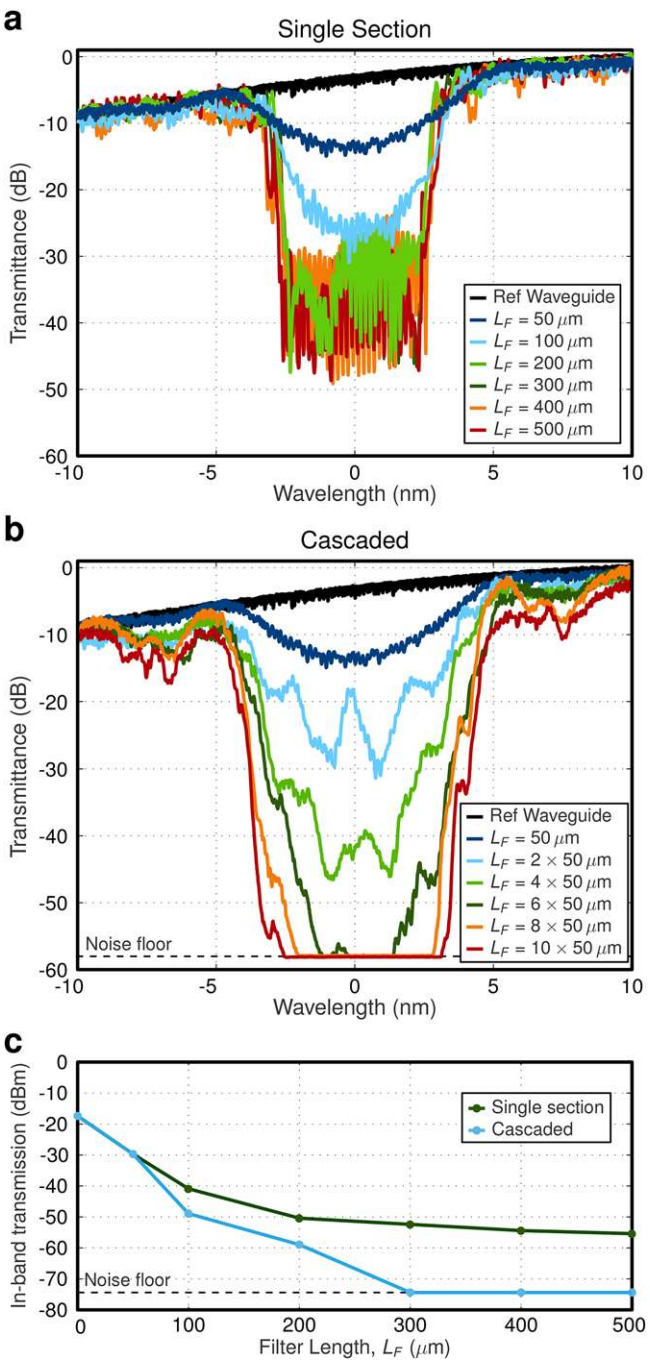

Figure 3. a,b) Measured transmission spectra of: a) single-section Bragg filters with increasing lengths, and b) proposed cascaded Bragg filter with fixed section length, of 50 µm, and number of sections ranging from 1 to 10. c) Comparison of in-band optical transmission as a function of filter length of single-section and proposed cascaded geometry, showing clear rejection saturation only for the single-section approach.

First, a series of single-section shifted Bragg gratings with different lengths were considered to illustrate the effect of optical rejection saturation. Rejection level is calculated as the difference between off-band transmission and the peak level inside the grating reflection band. As shown in **Figure 3**a, the rejection level

saturates near 40 dB for filter lengths beyond 300 µm. This weak rejection, compared with state-of-the-art Bragg filters,[17] may be attributed to errors in the electron-beam lithography and to the strong index contrast between silicon and air that accentuates the detrimental effect of fabrication imperfections. We compared the transmission of the filters to that of a reference strip waveguide to demonstrate the low-insertion loss of this kind of shifted geometry and show that the lower transmission at shorter wavelengths mainly arises from the response of the fiber-chip grating couplers.

The potential of our new approach for non-coherent cascading is shown by the characterization of a set of cascaded shifted Bragg gratings separated by single-mode waveguides. The cascaded filters have the same total lengths as the single-section structures shown in Figure 3a, but they are implemented by cascading multiple 50-µm-long grating sections. The 50 µm section length has been chosen just as an illustrative example, being the main conclusions valid for other section lengths. The single-mode waveguides have a width of 400 nm and a length of 20 µm. We use 25-µm-long tapers to make adiabatic transition between Bragg gratings and input and output single-mode waveguides. As depicted in Figure 1a, we included an S-bend (bending radius of 15 µm) between each two grating sections to promote radiation of any remaining power carried by the back-reflected first-order mode. The transmission spectra of the cascaded filters with total length ranging between 50 µm and 500 µm (comprising 10 sections of 50 µm length) are presented in Figure 3b. Figure 3c shows the transmission level within the rejection band as a function of the filter length for both single-section and cascaded configurations. The 0-filter-length point represents the transmission for a reference waveguide (without Bragg gratings). The proposed cascading approach yields a substantial increase in filter rejection, showing no clear evidence of saturation with the length. Note that for total lengths beyond 300 µm, the on-resonance transmission of the cascaded filter lies below the noise floor level of the automatic wavelength sweeping and detection system (CT400 from Yenista). The oscillations observed in some cascaded filters are attributed to random fabrication defects in the taper section that convert the second-order-mode reflection into the fundamental one and create some cavity effects. These imperfections may be attributed to local defects in the resist, for example, due to the presence of dust, or stitching errors in the electron beam lithography (3σ of 20 nm). The number of non-controlled errors may be minimized by fabricating the filters using industrial-like processes, for example, by multi-project wafers, and deep-UV lithography instead of electron-beam lithography.

In addition to a higher optical rejection, the cascaded filters exhibit a wider bandwidth. As discussed below, this wider rejection does not arise from relative wavelength shifts among different filter sections, but from the non-coherent nature of their interaction. From Equation (2) it follows that, for a given Bragg grating geometry (fixed n_g and κ), filter bandwidth decreases with the length. This could be qualitatively explained from the point of view of Fourier transform, as a longer spatial perturbation results in a narrower spectral response. However, different sections in the modal-engineered filter do not interact coherently. Thus, the bandwidth of the proposed filter is not determined by the total length, but by the length of the sections. This non-coherent interaction effect can be observed in Figure 3b, showing that

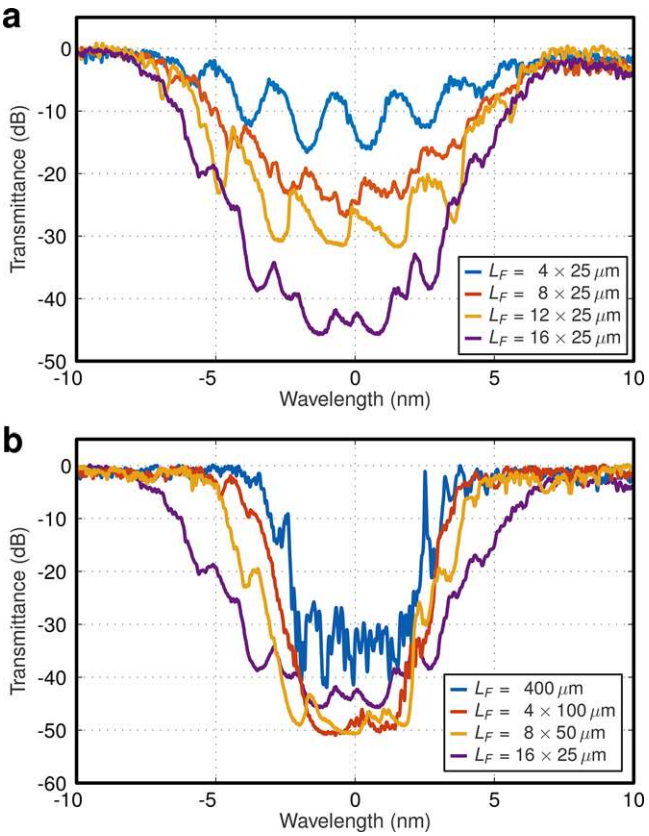

Figure 4. a,b) Measured transmission spectra of proposed cascaded filter for: a) fixed section length, of 25 µm, and increasing number of sections, showing no clear evidence of bandwidth increase with the number of sections, and b) fixed total filter length, of 400 µm, and decreasing section length. Filter bandwidth is determined by section length rather than by total length due to non-coherent cascading.

filters comprising 50-µm-long grating sections have a similar bandwidth, regardless of the total length.

Aiming at confirming the incoherent cascading in the proposed approach, we fabricated and characterized two different sets of filters. Note that while all the devices fabricated at the same time have a very repeatable response, for example, central wavelength, due to variations in the fabrication conditions the response of this new set of filters is not directly comparable with the ones shown in Figure 3. First, we fixed a section length of 25 µm and cascaded different number of sections, from 4 to 16, resulting in total filter lengths ranging between 100 µm and 400 µm. Measured spectra, shown in **Figure 4**a, demonstrate that the bandwidth of the cascaded filter does not significantly increase with an increasing number of sections. Hence, relative wavelength shifts can be discarded as the major reason for the wider bandwidth in the cascaded filters. Note that all the sections of the filter were placed close together in the chip, minimizing the effects of uneven silicon and resist thickness, while all sections in the same filter were written consecutively in the electron-beam lithography, minimizing beam current drifts over the time. Then, any deviation of the central Bragg wavelength was similar for all filter sections, yielding minimal relative shifts.

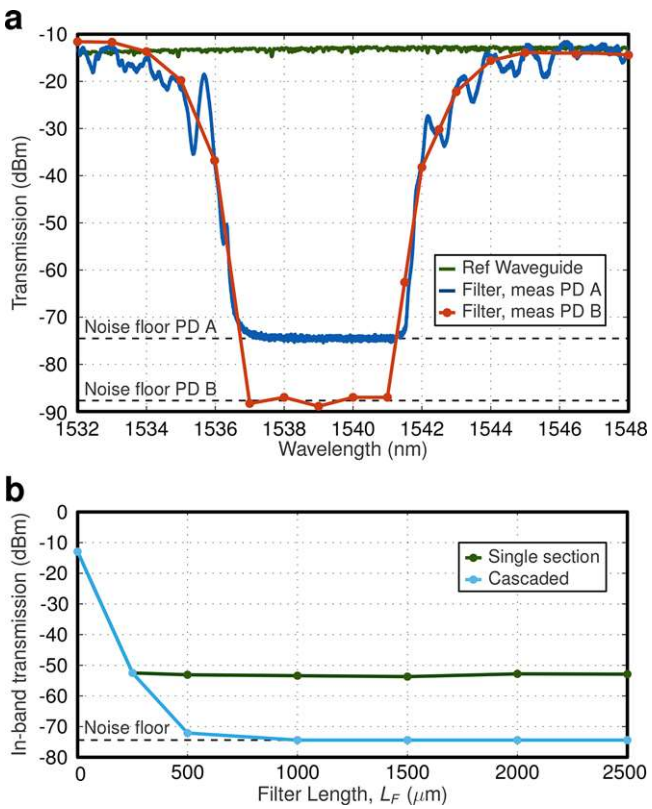

Figure 5. a) Transmission spectrum of cascaded shifted Bragg filter with total length of 2.5 mm, implemented by ten modal-engineered Bragg grating sections of 250 μm length. Measurements are performed with automatic wavelength sweep and detection system (CT400 form Yenista), PD A, and high-sensitivity photo-detector, PD B, in OSA (Anritsu MS9710B). Transmission of 3.5-mm-long strip waveguide is shown for comparison. b) Comparison of in-band optical transmission as a function of filter length of single-section and proposed cascaded geometry.

Then, we implemented the same total filter length, of 400 μm, by a single-section device, and by cascading 4, 6, and 8 sections of 100 μm, 50 μm, 25 μm lengths, respectively. The different measured spectra are presented in Figure 4b. It can be noticed that, even if the total filter length is always the same, the filter bandwidth increases with decreasing section length. These results clearly demonstrate the incoherent cascading in the proposed geometry, as the total filter bandwidth is mainly determined by the bandwidth of the individual Bragg gratings sections, rather than by the total filter length.

Finally, to demonstrate the remarkably large rejection capabilities of the proposed broken-coherency approach, we implemented a 2.5-mm-long filter, comprising 10 modal-engineered Bragg sections of 250 μm length. Rejection in single-section filters saturates after 300 μm length (see Figure 3). Thus, we choose a section length of 250 μm, below the saturation regime. The length of 2.5 mm is chosen to yield strong rejection. In this case, we used an optimized grating coupler design allowing a 5 dB improvement in the transmitted signal, compared to the previous examples. As shown in **Figure 5**a, the response of the filters was characterized using an automatic wavelength sweep and detection system (CT400 from Yenista) and the high-sensitivity photo-detector in OSA Anritsu MS9710B (see Section 2). For comparison, in Figure 5a, we also included the response of a reference strip waveguide of 3.5 mm length. This length includes the grating lengths (total of 2.5 mm), and the lengths of the input/output tapers S-bends and single-mode sections. The proposed filter exhibits negligible off-band insertion loss, within the variability determined by fiber alignment precision and fabrication tolerances. The Bragg on-resonance transmission level of the cascaded filter lies within the noise floor of the OSA, with (at least) 80 dB of on-chip optical rejection. This is, to the best of our knowledge, the largest rejection experimentally demonstrated for a silicon waveguide Bragg filter. Figure 5b compares the in-band transmission as a function of the filter length for the conventional and cascaded approach (with increasing number of grating sections with 250 μm length). It is worth noting that in the single-section case, the transmission decay saturates near 55 dBm (i.e., ≈40 dB rejection) for filter lengths beyond 300 μm. Hence, these results prove the potential of non-coherent cascading to increase filter rejection. In previous works, filter rejection achievable in a single chip was saturated near 60 dB level. This limitation was attributed to substrate scattering.[17,45] However, our filter shows a deeper rejection, without taking special care of this effect. Using the rejection of a single 250-μm-long section to fit the coupling coefficient in Equation (5), the filter with 10 cascaded sections would have a rejection near 300 dB. Still, such value might be compromised by imperfections like partial polarization rotation and radiation due to waveguide roughness. Nevertheless, the measurement of a deeper rejection would probably require more sensitive detectors and specific treatment of the substrate scattering. We used a fiber circulator at the input of the filter to collect all back-reflections. We retrieved a broadband and quasi-flat signal with no signature of the Bragg resonance and nearly −40 dBm level (mainly arising from reflections in gratings and backscattering in waveguide roughness). This result further confirms that Bragg back-reflections are effectively radiated away in the single-mode waveguide sections.

4. Conclusions and Outlook

In conclusion, we have proposed and experimentally demonstrated a new technology-independent strategy to preclude coherent interaction among nominally identical cascaded Bragg filters. This strategy provides a dramatic optical rejection increase, overcoming one of the major on-chip performance limitations. While maximum rejection level in conventional wavelength filters is seriously hampered by phase errors arising from fabrication imperfections, our approach allows effective cascading of low-rejection level stages without the need for any active tuning. High rejection levels have been demonstrated for cascaded MZIs[13] and ring resonators.[29] However, these devices required active tuning of each stage in the circuit to compensate phase errors. In some cases, sophisticated monitor and control algorithms need to be implemented to achieve and maintain a high rejection level.[13] Conversely, our approach yields high-rejection levels without any active control. This is a major advantage in terms of robustness, stability, and power consumption, especially when considering integration in complex circuits.

The innovative concept is to separate multimode Bragg grating sections by single-mode waveguides to break the coherency

of the interaction. We engineer the grating to yield Bragg back-reflections propagating in a high-order spatial mode, which is radiated away in the single-mode waveguides. This way, different filter sections are completely independent with no phase relationship, allowing effective optical rejection accumulation, even in the presence of phase errors. Based on this concept, we have experimentally demonstrated on-chip non-coherent cascading of multistage silicon Bragg filters, and have implemented a notch wavelength filter with an optical rejection higher than 80 dB. This is the largest optical rejection ever reported for an all-passive silicon photonic wavelength filter.

The approach proposed here can be translated to any other integrated photonic technology, as long as it allows the realization of multimode Bragg gratings and single-mode waveguides. Moreover, the concept could be applied to multi-corrugation geometries providing simultaneous Bragg resonances for both TE and TM modes[17] or to contra-directional couplers where reflected light is coupled to a different waveguide.[46,47] However, special care needs to be taken to fulfill conditions required to achieve coherent interaction suppression, thereby obviating multi-filter effects that can affect the spectrum of the filter.[47] While in the current configuration filtered light is radiated away, it can be easily collected in a different waveguide by means of a multimode directional coupler placed between the single-mode waveguide and the first grating section. Such asymmetric coupler can be engineered to yield effective coupling only between first-order mode of the input waveguide and fundamental mode of the output waveguide.[48] Hence, filtered light, propagating in the first-order mode of the waveguide can be collected. On the other hand, non-filtered light propagating in the fundamental mode would not be affected by this coupler.

The broken-coherency strategy proposed here releases new degrees of freedom to tailor the shape of on-chip wavelength filters. More specifically, the bandwidth of the cascaded Bragg filter is mainly determined by the length of the single section, while the rejection depth is set by the number of sections. Hence, previously reported strategies to reduce Bragg bandwidth, based on subwavelength engineering,[16,49] could be combined with the broken-coherency approach proposed here, allowing to simultaneously yield narrowband operation and ultra-high rejection. This unique capability to overcome bandwidth-rejection trade-off in conventional Bragg filters opens exciting opportunities for the development of efficient and fabrication tolerant Si wavelength filters, with a great potential for integrated nonlinear applications, for example, next generation Si-based photon-pair sources for quantum photonic circuits.

Acknowledgements

This work has been partially funded by the Agence Nationale de la Recherche (ANR-SITQOM-15-CE24-0005, ANR-MIRSPEC-17-CE09-0041) and the H2020 European Research Council (ERC) (ERC POPSTAR 647342). The fabrication of the device was performed at the Plateforme de Micro-Nano-Technologie/C2N, which is partially funded by the Conseil Général de l'Essonne. This work was partly supported by the French RENATECH network.

Keywords

Bragg gratings, optical filters, pump-rejection, silicon photonics

Received: August 31, 2018
Revised: February 28, 2019
Published online: July 15, 2019

[1] F. Boeuf, S. Crémer, E. Temporiti, M. Ferè, M. Shaw, C. Baudot, N. Vulliet, T. Pinguet, A. Mekis, G. Masini, H. Petiton, P. Le Maitre, M. Traldi, L. Maggi, *J. Light. Technol.* **2016**, *34*, 286.
[2] A. F. Gavela, D. G. García, J. C. Ramírez, L. M. Lechuga, *Sensors* **2016**, *16*, 285.
[3] S. Janz, D.-X. Xu, M. Vachon, N. Sabourin, P. Cheben, H. McIntosh, H. Ding, S. Wang, J. H. Schmid, A. Delge, J. Lapointe, A. Densmore, R. Ma, W. Sinclair, S.M. Logan, R. MacKenzie, Q.Y. Liu, D. Zhang, G. Lopinski, O. Mozenson, M. Gilmour, H. Tabor, *Opt. Express* **2013**, *21*, 4623.
[4] E. Knill, R. Laflamme, G. J. Milburn, *Nature* **2001**, *409*, 46.
[5] F. Mazeas, M. Traetta, M. Bentivegna, F. Kaiser, D. Aktas, W. Zhang, C. A. Ramos, L. A. Ngah, T. Lunghi, É. Picholle, N. Belabas-Plougonven, X. Le Roux, E. Cassan, D. Marris-Morini, L. Vivien, G. Sauder, L. Labonté, S. Tanzilli, *Opt. Express* **2016**, *24*, 28731.
[6] P. Cheben, J. H. Schmid, S. Wang, D.-X. Xu, M. Vachon, S. Janz, J. Lapointe, Y. Painchaud, M.-J. Picard, *Opt. Express* **2015**, *23*, 22553.
[7] M. Ziebell, D. Marris-Morini, G. Rasigade, J.-M. Fédéli, P. Crozat, E. Cassan, D. Bouville, L. Vivien, *Opt. Express* **2012**, *20*, 10591.
[8] L. Vivien, A. Polzer, D. Marris-Morini, J. Osmond, J.-M. Hartmann, P. Crozat, E. Cassan, C. Kopp, H. Zimmermann, J.-M. Fédéli, *Opt. Express* **2012**, *20*, 1096.
[9] P. Jouguet, S. Kunz-Jacques, A. Leverrier, P. Grangier, E. Diamanti, *Nat. Photonics* **2013**, *7*, 378.
[10] S. Azzini, D. Grassani, M. J. Strain, M. Sorel, L. G. Helt, J. E. Sipe, M. Liscidini, M. Galli, D. Bajoni, *Opt. Express* **2012**, *20*, 23100.
[11] W. C. Jiang, X. Lu, J. Zhang, O. Painter, Q. Lin, *Opt. Express* **2015**, *23*, 20884.
[12] D. Grassani, S. Azzini, M. Liscidini, M. Galli, M. J. Strain, M. Sorel, J. E. Sipe, D. Bajoni, *Optica* **2015**, *2*, 88.
[13] M. Piekarek, D. Bonneau, S. Miki, T. Yamashita, M. Fujiwara, M. Sasaki, H. Terai, M. G. Tanner, C. M. Natarajan, R. H. Hadfield, J. L. O'Brien, M. G. Thompson, *Opt. Lett.* **2017**, *42*, 815.
[14] N. C. Harris, D. Grassani, A. Simbula, M. Pant, M. Galli, T. Baehr-Jones, M. Hochberg, D. Englund, D. Bajoni, C. Galland, *Phys. Rev. X* **2014**, *4*, 041047.
[15] X. Wang, W. Shi, R. Vafaei, N. A. F. Jaeger, L. Chrostowski, *IEEE Photonics Technol. Lett.* **2011**, *23*, 290.
[16] D. Pérez-Galacho, C. Alonso-Ramos, F. Mazeas, X. Le Roux, D. Oser, W. Zhang, D. Marris-Morini, L. Labonté, S. Tanzilli, E. Cassan, L. Vivien, *Opt. Lett.* **2017**, *42*, 1468.
[17] C. Klitis, G. Cantarella, M. J. Strain, M. Sorel, *Opt. Lett.* **2017**, *42*, 3040.
[18] F. Xia, M. Rooks, L. Sekaric, Y. Vlasov, *Opt. Express* **2007**, *15*, 11934.
[19] P. Dong, N.-N. Feng, D. Feng, W. Qian, H. Liang, D. C. Lee, B. J. Luff, T. Banwell, A. Agarwal, P. Toliver, R. Menendez, T. K. Woodward, M. Asghari, *Opt. Express* **2010**, *18*, 23784.
[20] Y. Ding, M. Pu, L. Liu, J. Xu, C. Peucheret, X. Zhang, D. Huang, H. Ou, *Opt. Express* **2011**, *19*, 6462.
[21] F. Horst, W. M. J. Green, S. Assefa, S. M. Shank, Y. A. Vlasov, B. J. Offrein, *Opt. Express* **2013**, *21*, 11652.
[22] J. Wang, I. Glesk, L. R. Chen, *Electron. Lett.* **2015**, *51*, 712.
[23] Z. Zou, L. Zhou, M. Wang, K. Wu, J. Chen, *Opt. Express* **2016**, *24*, 12831.
[24] Z. Lu, J. Jhoja, J. Klein, X. Wang, A. Liu, J. Flueckiger, J. Pond, L. Chrostowski, *Opt. Express* **2017**, *25*, 9712.

[25] A. M. Vengsarkar, P. J. Lemaire, J. B. Judkins, V. Bhatia, T. Erdogan, J. E. Sipe, *J. Light. Technol.* **1996**, *14*, 58.
[26] N. M. Litchinitser, B. J. Eggleton, G. P. Agrawal, *J. Light. Technol.* **1998**, *16*, 1523.
[27] F. Ouellette, *Opt. Lett.* **1987**, *12*, 847.
[28] J. St-Yves, H. Bahrami, P. Jean, S. Larochelle, W. Shi, *Opt. Lett.* **2015**, *40*, 5471.
[29] J. R. Ong, R. Kumar, S. Mookherjea, *IEEE Photonics Technol. Lett.* **2013**, *25*, 1543.
[30] M. L. Cooper, G. Gupta, M. A. Schneider, W. M. J. Green, S. Assefa, F. Xia, Y. A. Vlasov, S. Mookherjea, *Opt. Express* **2010**, *18*, 26505.
[31] J.-M. Liu, *Photonic Devices*, Cambridge University Press, Cambridge, UK **2009**.
[32] M. W. Pruessner, T. H. Stievater, W. S. Rabinovich, *Opt. Lett.* **2007**, *32*, 533.
[33] Y. Painchaud, M. Poulin, C. Latrasse, M.-J. Picard, presented at *Int. Conf. on Group IV Photonics*, IEEE, San Diego, CA, USA, August **2012**, pap. 13058915.
[34] W. Zhang, N. Ehteshami, W. Liu, J. Yao, *Opt. Lett.* **2012**, *40*, 3153.
[35] FDTD solutions, Lumerical Solutions, Inc., http://www.lumerical.com.
[36] A. Yariv, *IEEE J. Quantum Electron.* **1973**, *9*, 919.
[37] X. Wang, Y. Wang, J. Flueckiger, R. Bojko, A. Liu, A. Reid, J. Pond, N. A. F. Jaeger, L. Chrostowski, *Opt. Lett.* **2014**, *39*, 5519.
[38] H. Qiu, J. Jiang, P. Yu, T. Dai, J. Yang, H. Yu, X. Jiang, *Opt. Lett.* **2016**, *41*, 2450.
[39] P. Cheben, R. Halir, J. H. Schmid, H. A. Atwater, D. R. Smith, *Nature* **2018**, *560*, 565.
[40] A. D. Simard, N. Belhadj, Y. Painchaud, S. LaRochelle, *IEEE Photonics Technol. Lett.* **2012**, *24*, 1033.
[41] X. Wang, W. Shi, H. Yun, S. Grist, N. A. F. Jaeger, L. Chrostowski, *Opt. Express* **2010**, *20*, 15547.
[42] R. Halir, P. Cheben, S. Janz, D.-X. Xu, I. Molina-Fernández, J. G. Wangüemert-Pérez, *Opt. Lett.* **2009**, *34*, 1408.
[43] D. Benedikovic, P. Cheben, J. H. Schmid, D.-X. Xu, B. Lamontagne, S. Wang, J. Lapointe, R. Halir, A. Ortega-Moux, S. Janz, M. Dado, *Opt. Express* **2015**, *23*, 22628.
[44] Y. Zhang, Y. He, J. Wu, X. Jiang, R. Liu, C. Qiu, X. Jiang, J. Yang, C. Tremblay, Y. Su, *Opt. Express* **2016**, *24*, 6586.
[45] G. Cantarella, C. Klitis, M. Sorel, M. J. Strain, *Opt. Express* **2017**, *25*, 19711.
[46] H. Qiu, G. Jiang, T. Hu, H. Shao, P. Yu, J. Yang, X. Jiang, *Opt. Lett.* **2012**, *38*, 1.
[47] M. Hammood, A. Mistry, M. Ma, H. Yun, L. Chrostowski, N. A. F. Jaegerh, *Opt. Lett.* **2019**, *44*, 439.
[48] J. Wang, S. He, D. Dai, *Laser Photonics Rev.* **2014**, *8*, L18.
[49] D. Oser, D. Pérez-Galacho, C. Alonso-Ramos, X. Le Roux, S. Tanzilli, L. Vivien, L. Labont, E. Cassan, *Opt. Lett.* **2018**, *43*, 3208.